

Supporting information

1. Structural response to pressure

The crystal structures of NM and NNHT (each unit cell contains four molecules) are shown in Fig. S1, where (a) and (b) are the crystal structure and unimolecular configuration of NM, (c) and (d) (a plan view taken from the c-axis direction) are both crystal structures of NNHT. NM and NNHT belong to orthorhombic ($P2_12_12_1$, 19) [1] and monoclinic ($P2_1/a$, 14) [2], respectively. Fig. S1 (d) and (e) show that the structure of NNHT is different from the simple molecular structure of NM containing only one methyl group and one nitro group. Its single molecule has a "chair"-like configuration, which contains two methylene groups, CN alternately connected rings, NN single bond and C=N double bond. The inclusion of double bonds and rings suggests that NNHT has higher energy properties than NM. In addition, the intermolecular hydrogen bonding of NM is weaker than that of NNHT.

The lattice parameters of NM and NNHT in the published papers and our calculated results are shown in Table S1. At zero pressure, our calculated parameters of NM are compared with experimental data for neutron scattering [1], indicating that other calculations [3,4-8] are less as accurate as ours. As shown by the calculation results in refs. [3-5], the calculated results of DFT without dispersion correction are far from the experimental results. In addition, the maximum error of the NNHT lattice parameters we calculated using GGA-PBE-G is less than 2.6%. [8]. Compared with TS correction, G correction is better, so the whole paper adopts GGA-PBE-G for simulation. Therefore, our calculation results are reliable [9].

To explore the triggering mechanism of EMs under pressure effect, we pressurized NM and NNHT to the range of explosion pressure of about 13 GPa [10] and 30 GPa [11], respectively. Their sensitivity-related bandgap values [12] are shown in Figs. S2 (c) (NM) and (f) (NNHT) as a function of pressure, both of which appear to decrease gradually with pressure, showing that they become more sensitive under the action of pressure [12]. In Fig. S2 (a), we can see that our calculated NM lattice parameters as a function of pressure are in good agreement with the experimental values [13,14] within 11 GPa. However, around 11-12 GPa, our calculated lattice constants mutate. This is consistent with the result of experiments [14], where a new phase is produced at 11 GPa. Moreover, our results are supported by the work of Appalakondaiah et al. [3]. They used the GGA-PBE-G06 simulation results to find that the lattice constants undergone a similar mutation at 10-12 GPa. Figures S2 (b) and (c) also show the abrupt change in volume and bandgap between 11 and 12 GPa. Figures S2 (d), (e) and (f) are the lattice constants, volume and angle β of NNHT, which all decrease gradually with increasing pressure. The lattice parameters a and b are very close to each other at 0-3 GPa.

To further understand their high-pressure behaviors, we plot the evolution of the X-ray diffraction patterns under pressure in Fig. S3. Fig. S3 (a) is the X-ray diffraction pattern of NM. It can be found that there is a significant change in the 11-12 GPa pattern. After 12 GPa, a small peak is generated at $2\theta=22.1^\circ$, explaining that a phase transition occurs at 11-12 GPa. As shown in Fig. S3 (b), NNHT generate a new peak at $2\theta=25.2^\circ$ at 1 GPa, and the peak become weaker after 2 GPa. In addition, at

20 GPa, a new peak is also generated at about $2\theta=35.9^\circ$. Therefore, we believe that the phase transition may occur in NNHT at 0-1 GPa and 17-20 GPa. Finally, the bandgap value of NNHT exhibits a small fluctuation at 3 GPa with increasing pressure, and then resumes a gradually decreasing trend.

2. Vibration modes and frequencies of NM and NNHT

Table S2 is the comparison results between the experimental [15] and calculated [3,4] values of the vibration modes and frequencies of NM. The results show that the lower frequencies are in good agreement with the experimental values, and the gap is larger at high frequencies. Our results are in good agreement with the results of the literature [3]. Reference [4] does not use the correction, which is the reason for the large gap with it. The modes with Raman activity are shown in the table.

Table S3 is the vibration modes and frequencies of the NNHT. There are no other calculations and experiments. The vibrational modes with Raman activity are listed.

Fig. S4 shows the results of the evolution of the vibration mode with pressure for NM and NNHT. As shown in Fig. S4, it is the result of the evolution of the NM vibration mode with pressure (peak position $> 400 \text{ cm}^{-1}$), which contains a total of 14 internal vibration units, and each mode contains four vibration modes [3]. This paper adopts the naming method of literatures [3,4]. The specific vibrations are shown in Table S2. The NM has a total of 56 modes at the Gamma (G) point, and at zero pressure, 48 modes are Raman-active (unmarked vibration assignments are not

Raman-active). Their irreducible representation in the first Brillouin zone is $14A_g(R) + 11B_{1g}(R+I) + 11B_{2g}(R+I) + 12B_{3g}(R+I)$. Here, R and I represent Raman and infrared activity, respectively. The vibrational modes we calculated using GGA-PBE-G are in good agreement with experimental values [15] and other calculations [3,4]. The difference is that at 475.1-475.5 cm^{-1} , we can see not only NO_2 rocking, but also CH_3 rocking. This is slightly different from previous literatures [3,4] with only CH_3 rocking. Returning to Fig. S4, we can see that all vibrational modes have abrupt changes at 11-12 GPa. Similar to the discontinuous change of 10-12 GPa in the literature [3]. But it has different results from the literature [4]. It is worth noting that [4] did not use the van der Waals correction. Combining parts of the structure (see the appendix), we believe that an isostructural phase transition occurs at 11-12 GPa. This is consistent with the study of the experiment [14], under the effect of high pressure until the melting value 27.3 GPa, which always maintains the structure of P212121. The main reason is the change in the angle of C-N-O described in the literature [3]. After 12 GPa, the frequencies of all vibration modes continued to increase. The frequency distribution range becomes wider, and the peak width corresponding to the actual Raman peak increases. Unlike NM, NNHT has no obvious distinction between intramolecular and intermolecular vibrational modes, and we also study vibrational modes $>400 \text{ cm}^{-1}$. There are four vibrational modes A_g , B_g , A_u and B_u in NNHT. At 0GPa, there are 81 Raman-active vibrational modes of $42A_g(R) + 39B_g(R)$, while A_u and B_u have no Raman activity at all (not listed). The details are listed in Table S3. Unfortunately, there is no Raman spectroscopy study of NNHT in the experiment.

This article is the first time to study its Raman correlation. NNHT is much more complicated than NM, and the evolution of vibration mode with pressure is shown in Fig. S4, which does not show a more perfect linear change like NM. Similar to NM, every two modules form a 'unit', denoted as M. It can be seen that in a low pressure region 0-2GPa, M1, M2, M3, M5, M9, M13, M14, M15, M19 and M33 contain discontinuous changes in the vibration modes. So, we infer that it may be a phase transition around 1GPa. M4, M7, M10, M11, M12, M16, M29 and M30 at 0-3 GPa, 3-17 GPa, and 17-30 GPa were clearly divided into three different slopes, indicating that NNHT may have three phases transformation at 0-30 GPa. M18, M20, M21, M23, M27, M28, M36, M38, M39, M40, M41 and M42 showed almost the same trend in 0-30GPa. In addition, the modes included in M5, M6 and M37 exhibit softening in different pressure ranges. It is worth noting that we have not found relevant experimental studies to support this. Fortunately, phonons play an important role in the study of phase transitions [16,17]. When the imaginary frequency appears, it indicates that the crystal is unstable and is transitioning to a stable phase. Also, no experiments have loaded and published NNHT pressures from 0-30 GPa. Based on this, we calculate the corresponding phonon spectrum and make predictions. As shown in Fig. S6, under 0 GPa, NNHT has no imaginary frequency and the structure is stable. When the pressure is 1 GPa, an imaginary frequency (-45.5 cm^{-1}) appears at the G point. There is also an imaginary frequency (over -50 cm^{-1}) at 2 GPa, although there is no imaginary frequency at the G point. Continuing to see, 15-17 GPa produces imaginary frequencies of -61.4 and -56.3 cm^{-1} at the G point, respectively.

The generation of sufficiently large imaginary frequencies [18] can indicate that NNHT may have phase transitions between 1-2 GPa and 15-17 GPa. This is generally consistent with the analysis in the appendix. Fig. S7 shows the molecular changes of the NNHT structure in the crystal under the action of pressure, and the bending of C-N-NO₃ becomes more and more obvious under the action of pressure. Gradually change from a 'chair' shape to a 'Z' shape. Except at 0 GPa, no imaginary frequency is generated at other pressure points, indicating that they are all stable. A key issue is also illustrated from here, Raman spectroscopy is sufficiently sensitive, but specific changes produced by vibrational modes do not necessarily induce phase transitions.

As shown in Fig. S5 (a), the specific vibration states of the M4, M5, M6, M8, M10, M12, M13 and M14 vibration mode units of NM are listed. The symbols next to it indicate specific vibration modes (A, B₁, B₂ and B₃). The C-H, C-N, etc. vibrations can be clearly distinguished. Similarly, Figures S5 (b) and (c) represent the relevant information of NNHT.

3. Bond dissociation energies of NM and NNHT partial bonds

Table S4 shows the bond dissociation energies of NM and NNHT, where they may be trigger bonds. It contains experimental values [4,19] and calculated values [1,2,25], which are compared to our results. The corresponding value is clear at a glance.

The C-N, C-H, N-O bond lengths and partial bond dissociation energies (BDEs) of NM are listed in Table S4. The bond dissociation energy (BDE) of a substance R-X

generally refers to the reaction enthalpy change of the chemical bond breaking process, which reflects the energy required for the bond breaking process [20]. The bond lengths we calculated using both methods are in good agreement with other calculations [4,20] and experiments [1]. The BDE of NM calculated using the semi-empirical exchange correlation functional B3LYP and correction using G [21, 22, 23, 24]. The calculated BDE for C-N is 62.792 kcal/mol, which is slightly larger than the 56.4 kcal/mol in the literature [19], but closer to the experimental value of 60.8 kcal/mol [25]. Furthermore, we calculated the dissociation energy of the longest C-H₃ in CH₃ to be 98.968 kcal/mol. The bond energy of the longest N-O bond is 123.183 kcal/mol. Using the same method, the longest N-N, C-N, C-H, N-H and N-O bond energies in the NNHT molecule were calculated to be 36.068, 50.079 (50.080), 61.196, 102.515 and 105.279 kcal/mol, respectively.

4. Phonon spectrum of NNHT

Fig. S6 shows the phonon spectrum of NNHT under pressure. It can be clearly seen that there are imaginary frequencies at 1GPa, 2GPa, 15GPa and 17GPa respectively.

5. Crystal structure of NNHT under pressure

The crystal structures of NNHT under the action of 0, GPa, 1GPa, 2GPa, 15GPa and 17GPa pressures projected along the YZ plane are shown in Fig. S7. The red circle represents the molecular response of NNHT to pressure.

6. The p_k of NM and NNHT varies with pressure.

Figures S8 and S9, respectively, are the cells whose p_k gradually increases with the pressure change after the phase transition.

7. Comparison of the initial reaction pathways of NM and NNHT with traditional trigger bond cleavage

As shown in Fig. S10, the location distribution of possible reactions among the three NM molecules and the degree of difficulty of reactions. Numerically, the energy barrier order of the first intramolecular H transfer is (1) 63.199kcal/mol> (2) 63.507kcal/mol> (3)99.899kcal/mol. Therefore, we think (1) has the most advantages.

References

- [1] S.F. Trevino, E. Prince, C.R. Hubbard, Refinement of the structure of solid nitromethane, *The Journal of Chemical Physics*, 1980, 73, 2996-3000.
- [2] A.J. Bracuti, Crystal structure of 2-nitrimino-5-nitro-hexahydro-1,3,5-triazine, *Journal of Chemical Crystallography*, 2004, 34, 135-140.
- [3] S. Appalakondaiah, G. Vaitheeswaran, S. Lebègue, A DFT study on structural, vibrational properties, and quasiparticle band structure of solid nitromethane, *The Journal of Chemical Physics*, 2013, 138, 184705.
- [4] H. Liu, J. Zhao, D. Wei, Z. Gong, Structural and vibrational properties of solid nitromethane under high pressure by density functional theory, *The Journal of Chemical Physics*, 2006, 124, 124501.
- [5] J. Chang, X. Zhou, G. Zhao, L. Wang, A first-principles study of the structural,

electronic and elastic properties of solid nitromethane under pressure, *Science China Physics, Mechanics and Astronomy*, 2013, 56, 1874-1881.

[6] D.C. Sorescu, B.M. Rice, D.L. Thompson, Theoretical studies of solid nitromethane, *The Journal of Physical Chemistry B*, 2000, 104, 8406-8419.

[7] F. Guo, X.L. Cheng, H. Zhang, Reactive molecular dynamics simulation of solid nitromethane impact on (010) surfaces induced and nonimpact thermal decomposition, *The Journal of Physical Chemistry A*, 2012, 116, 3514-3520.

[8] M. Zhong, H. Qin, Q.J. Liu, C.L. Jiang, F. Zhao, H.L. Shang, F.S. Liu, B. Tang, A systematic study of the surface structures and energetics of CH₃NO₂ surfaces by first-principles calculations, *Journal of Molecular Modeling*, 2019, 25, 164.

[9] F.L. Yarger, B. Olinger, Compression of solid nitromethane to 15 GPa at 298 K, *The Journal of Chemical Physics*, 1986, 85, 1534-1538.

[10] S. Courtecuisse, F. Cansell, D. Fabre, J.P. Petitet, Comparative Raman spectroscopy of nitromethane- h₃, nitromethane- d₃, and nitroethane up to 20 GPa, *The Journal of Chemical Physics*, 1998, 108, 7350-7355.

[11] W. Wang, S.M. Han, D.L. Zhang, J.B. Liu, B. Wang, J.Q. Xue, B.K. Shang, Research progress of insensitive energetic material NNHT, *Chemical Propellants & Polymeric Materials*, 2020, 18, 1-8.

[12] W. Zhu, J. Xiao, G. Ji, F. Z, H. Xiao, First-Principles Study of the Four Polymorphs of Crystalline Octahydro-1,3,5,7-tetranitro-1,3,5,7-tetrazocine, *The Journal of Physical Chemistry B*, 2007, 111, 12715-12722.

[13] D.T. Cromer, R.R. Ryan, The structure of nitromethane at pressures of 0.3 to 6.0

- GPa, *The Journal Physics Chemistry*, 1985, 89, 2315-2318.
- [14] M. Citroni, F. Datchi, R. Bini, M.D. Vaira, P. Pruzan, B. Canny, V. Schettino, Crystal structure of nitromethane up to the reaction threshold pressure, *The Journal of Physical Chemistry B*, 2008, 112, 1095-1103.
- [15] R. Ouillon, J.P. Pinan-Lucarré, P. Ranson, G. Baranovic, Low-temperature Raman spectra of nitromethane single crystals Lattice dynamics and Davydov splittings, *The Journal of Chemical Physics*, 2002, 116, 4611-4625.
- [16] H. Moriwake, A. Kuwabara, C.A.J. Fisher, H. Taniguchi, M. Itoh, I. Tanaka, First-principles calculations of lattice dynamics in CdTiO₃ and CaTiO₃: Phase stability and ferroelectricity, *Physical Review B*, 2011, 84, 104114.
- [17] A. Togo, I. Tanaka, First principles phonon calculations in materials science, *Scripta Materialia*, 2015, 108, 1-5.
- [18] J. Shao, X. Cheng, X. Yang, Density functional calculations of bond dissociation energies for removal of the nitrogen dioxide moiety in some nitroaromatic molecules, *Journal of Molecular Structure: THEOCHEM*, 2005, 755, 127-130.
- [19] X. Su, X. Cheng, Y. Liu, Q. Li, Theoretical calculation of bond dissociation energies and heats of formation for nitromethane and polynitromethanes with density functional theory international, *Journal of Quantum Chemistry*, 2007, 107, 515-521.
- [20] Y. Liu, J. Zhang, K. Wang, J. Li, Q. Zhang, J.M. Shreeve, Bis(4-nitraminofurazanyl-3-azoxy)azofurazan and derivatives: 1,2,5-Oxadiazole structures and high-performance energetic materials, *Angewandte Chemie International Edition*, 2016, 55, 1-5.

- [21] A.D. Becke, A multicenter numerical integration scheme for polyatomic molecules, *The Journal of Chemical Physics*, 1988, 88, 2547-2553.
- [22] C. Lee, W. Yang, R.G. Parr, Development of the Colic-Salvetti correlation-energy formula into a functional of the electron density, *Physical Review B*, 1988, 37, 786-789.
- [23] A. Tkatchenko, M. Scheffler, Accurate molecular Van Der Waals interactions from ground-state electron density and free-atom reference data, *Physical Review Letter*, 2009, 102, 073005.
- [24] S. Grimme, Semiempirical GGA-Type Density Functional Constructed with a Long-Range Dispersion Correction, *Journal of Computational Chemistry*, 2006, 27, 1787-1799.
- [25] Y.R. Luo, *Handbook of Bond Dissociation Energies in Organic Compounds* (CRC Press: Boca Raton, 2003).

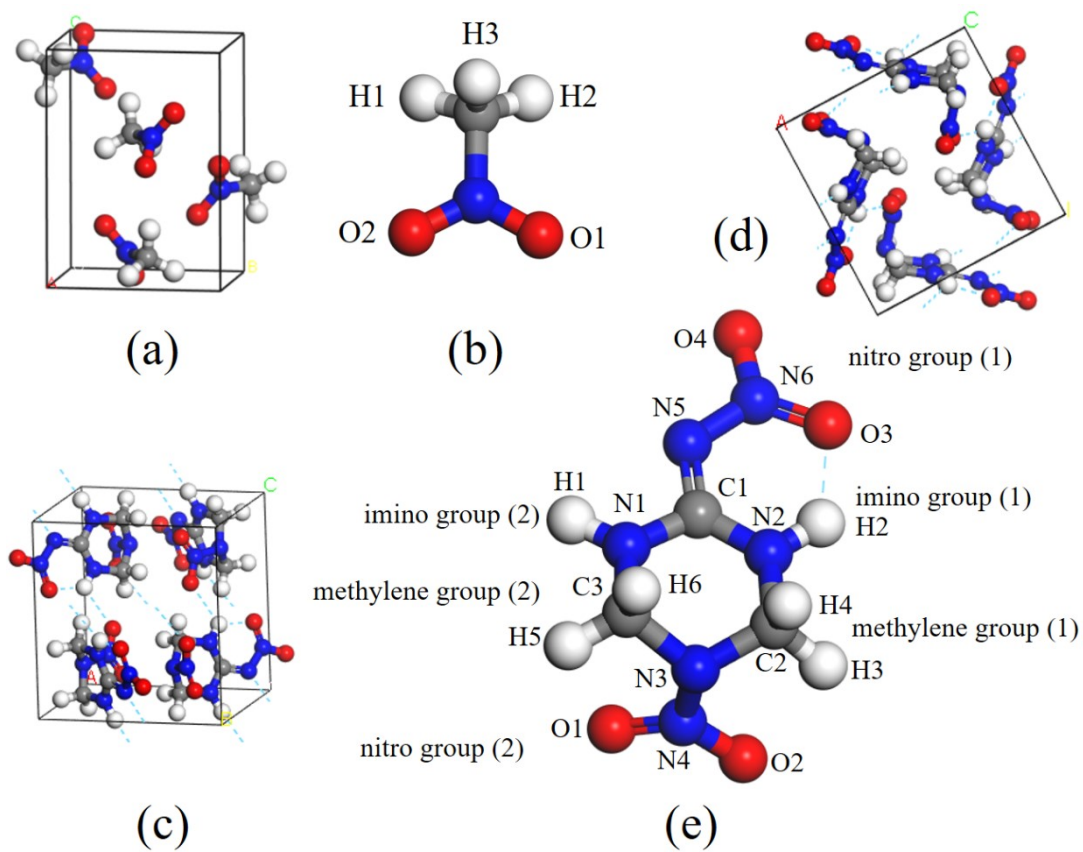
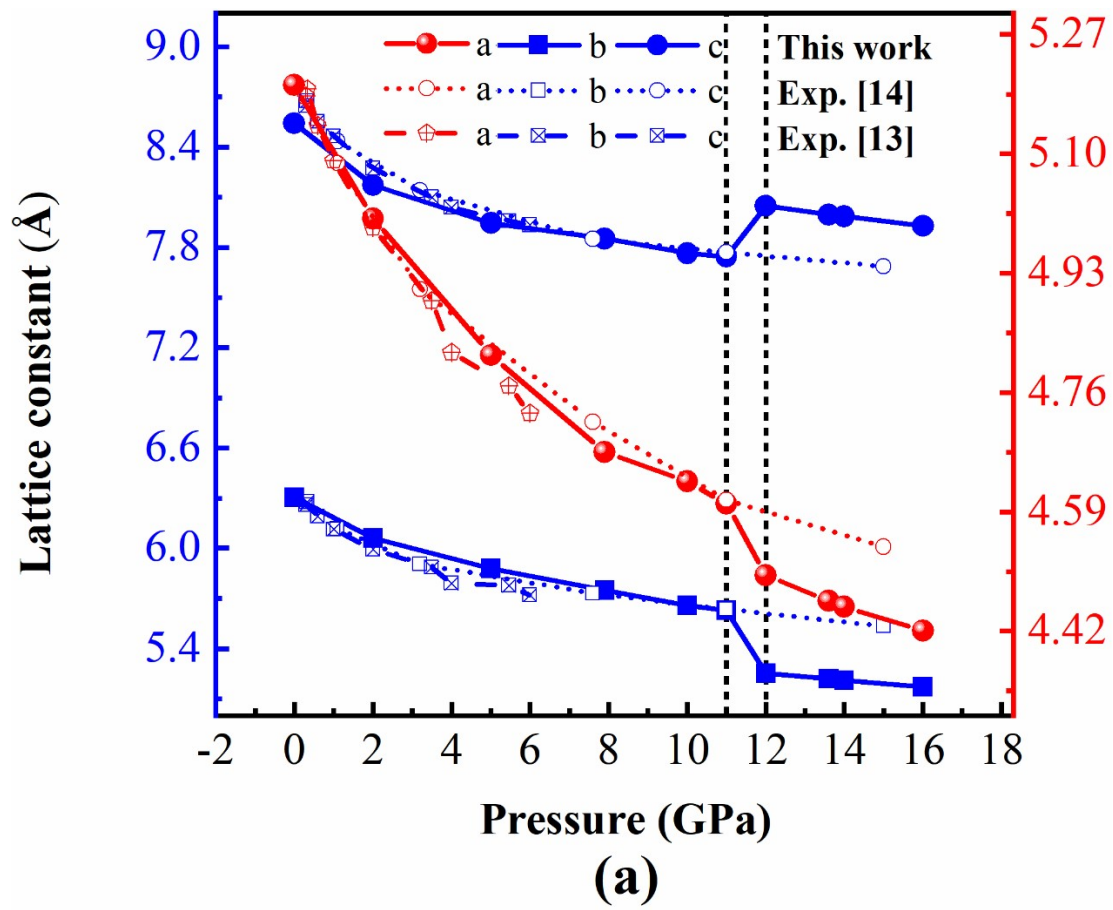
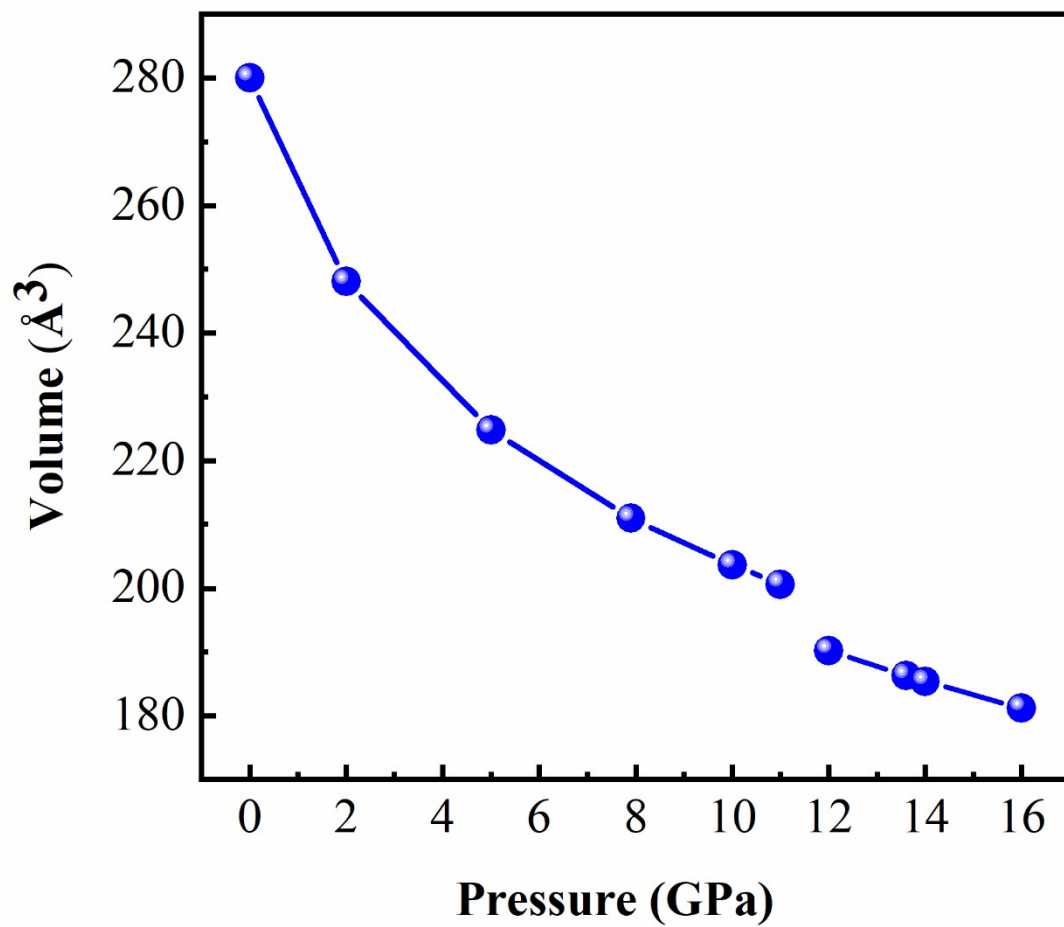
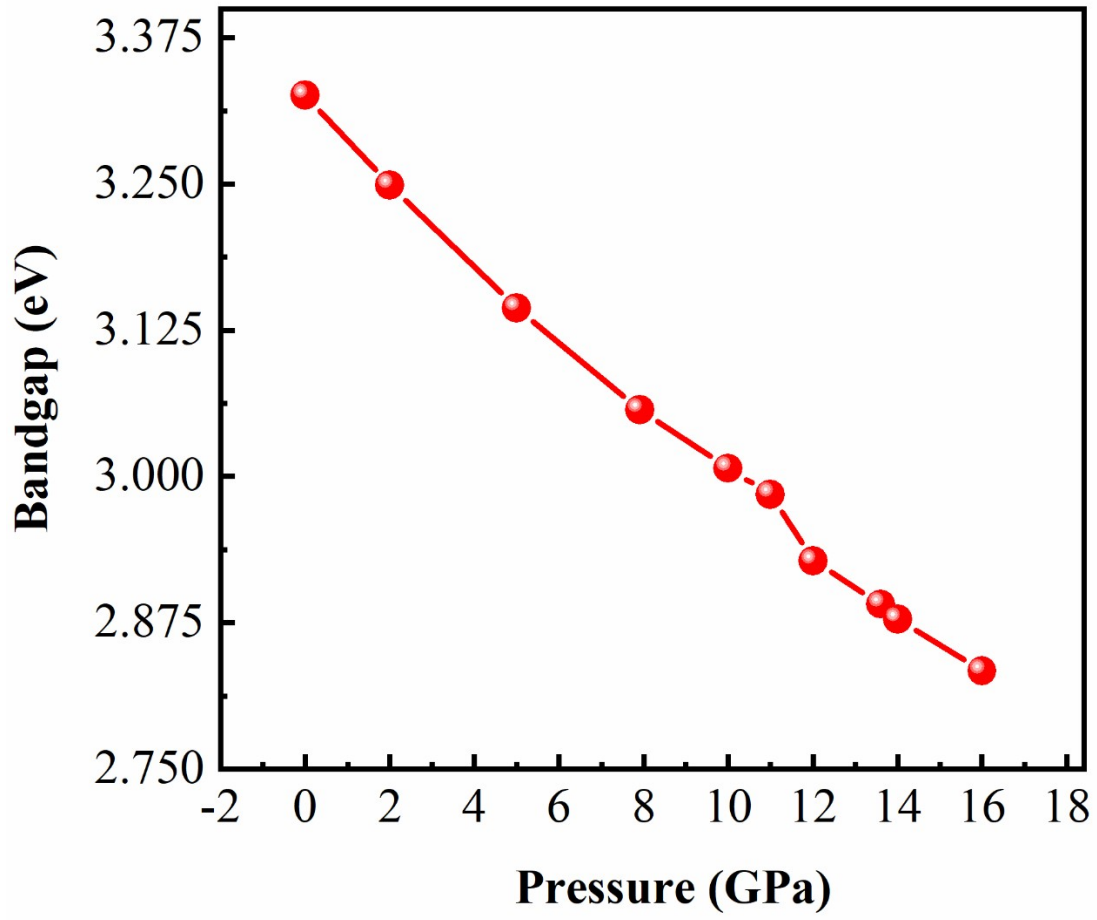


Fig. S1. Crystal and single-molecule structures of NM and NNHT.

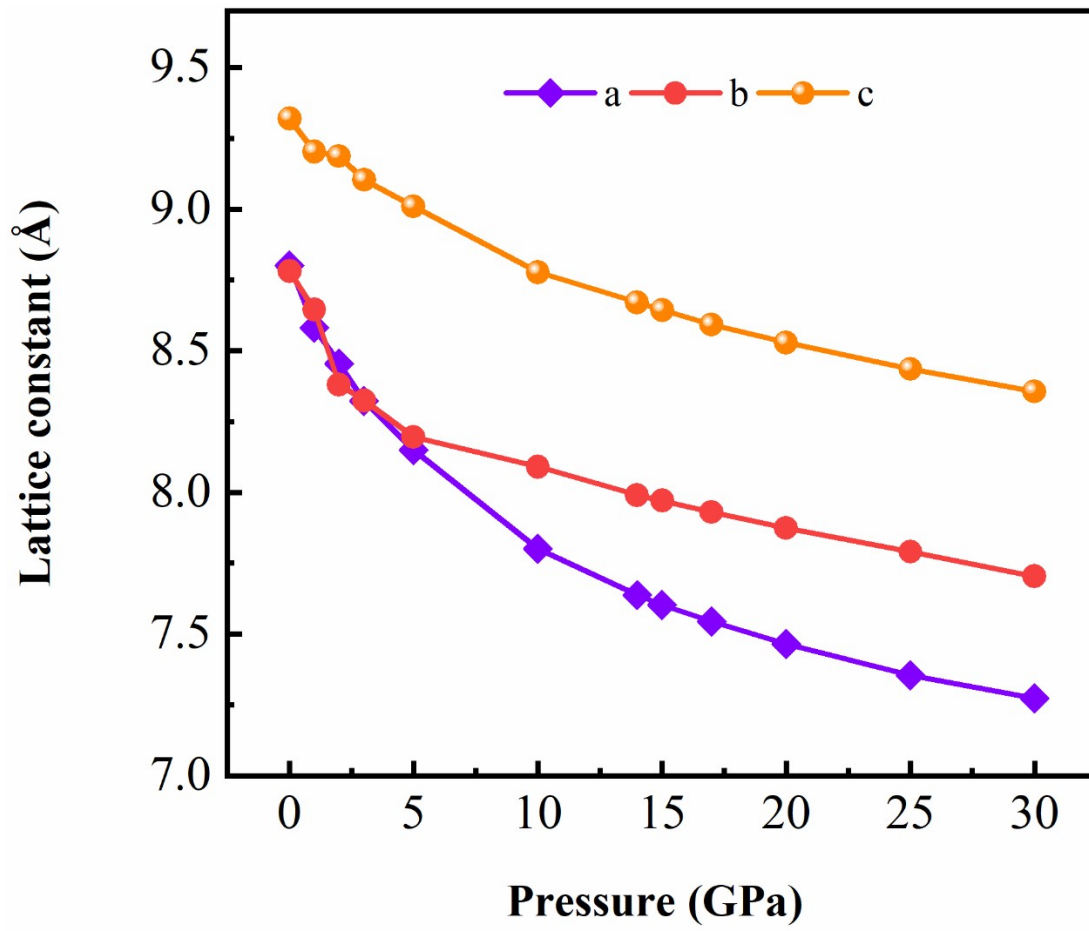




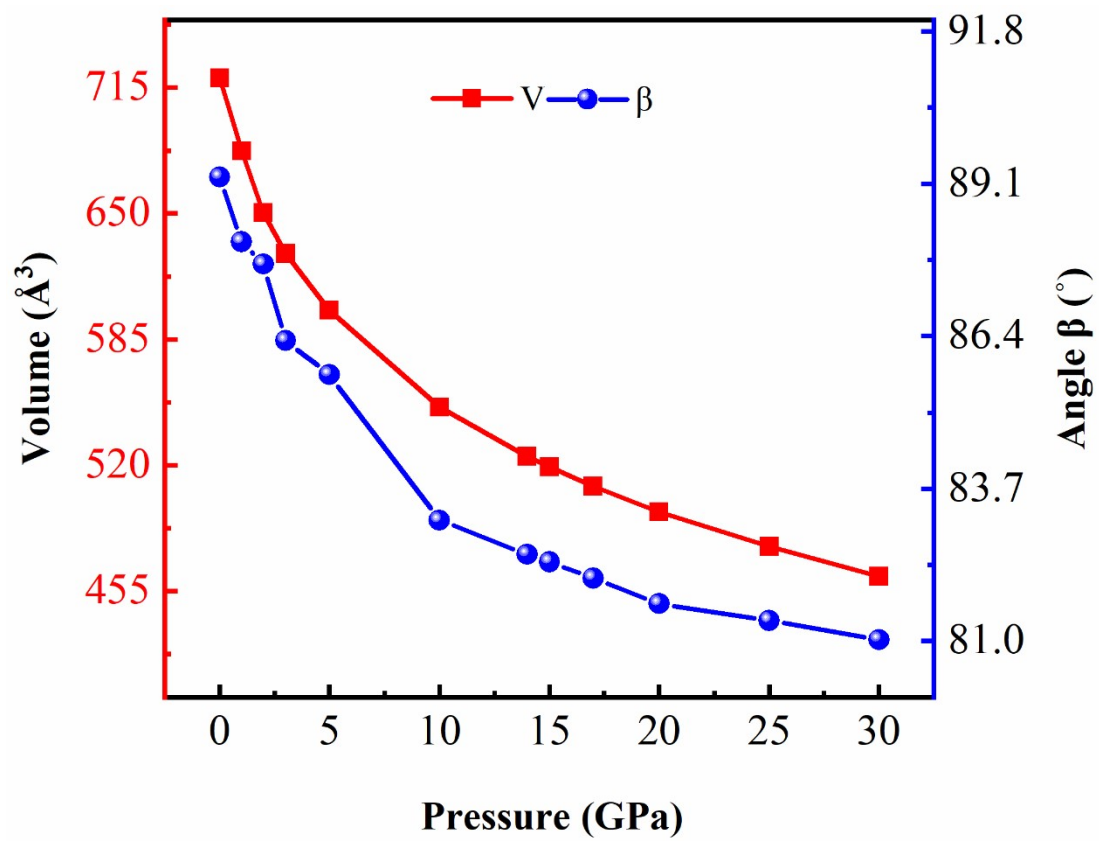
(b)



(c)



(d)



(e)

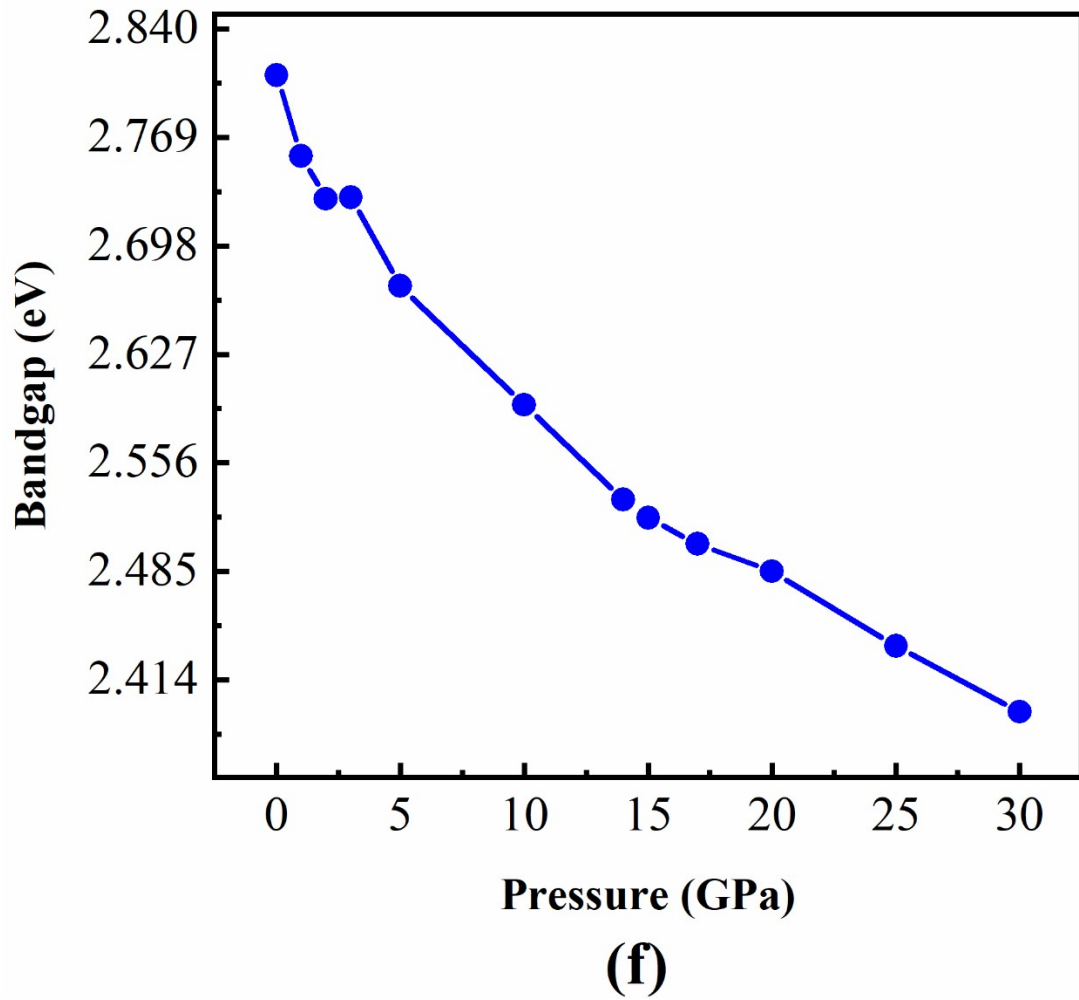
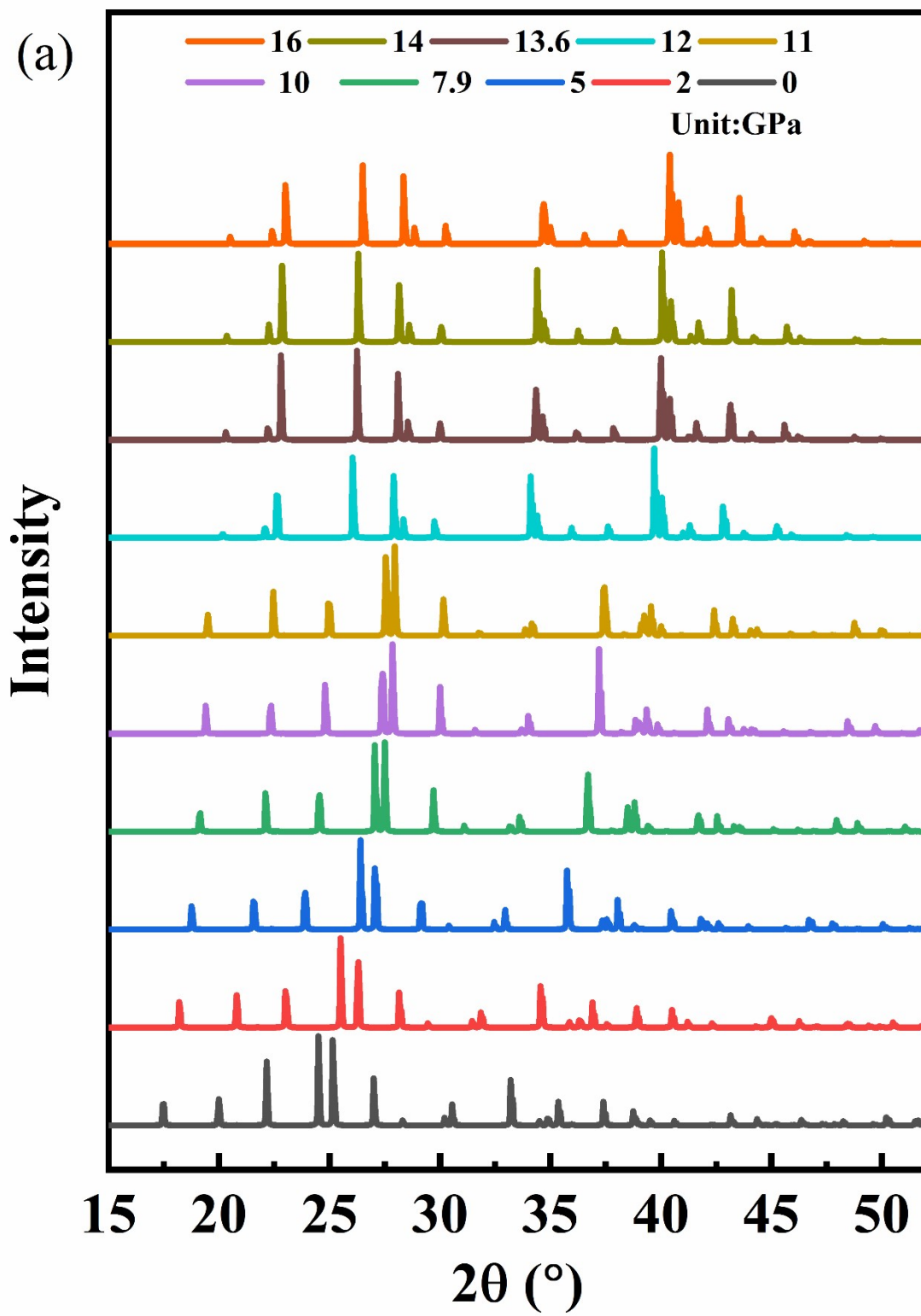


Fig. S2. Crystal parameters and bandgaps of NM and NNHT as a function of pressure, respectively. (a), (b) and (c) belong to NM, (d), (e) and (f) are NNHT.



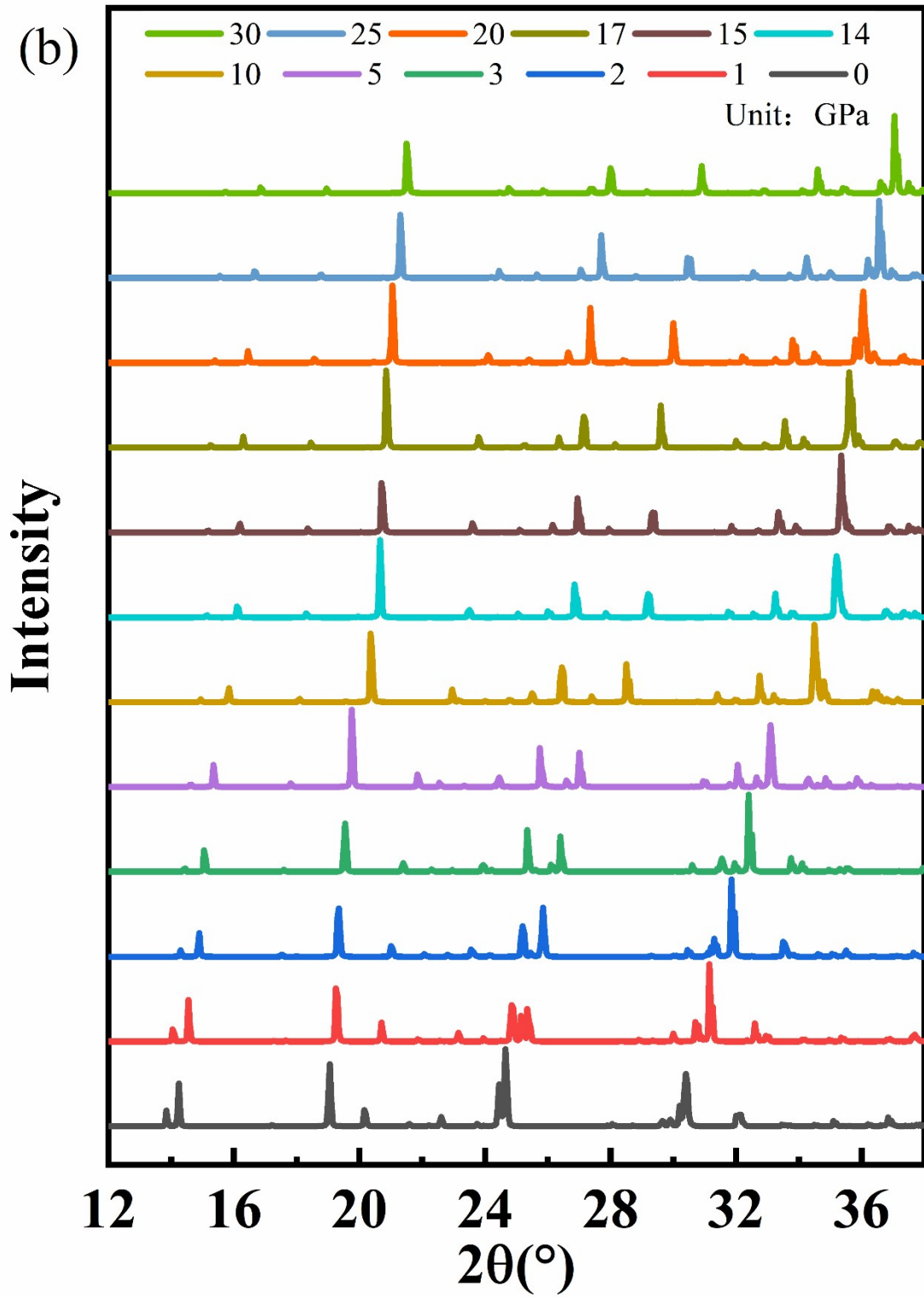
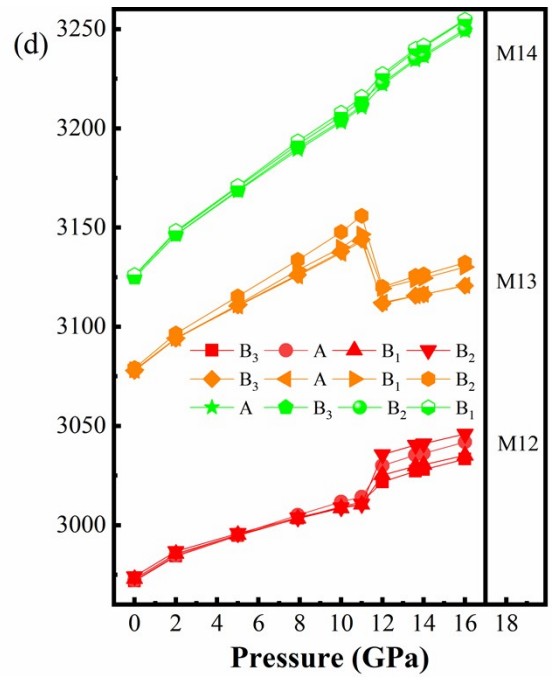
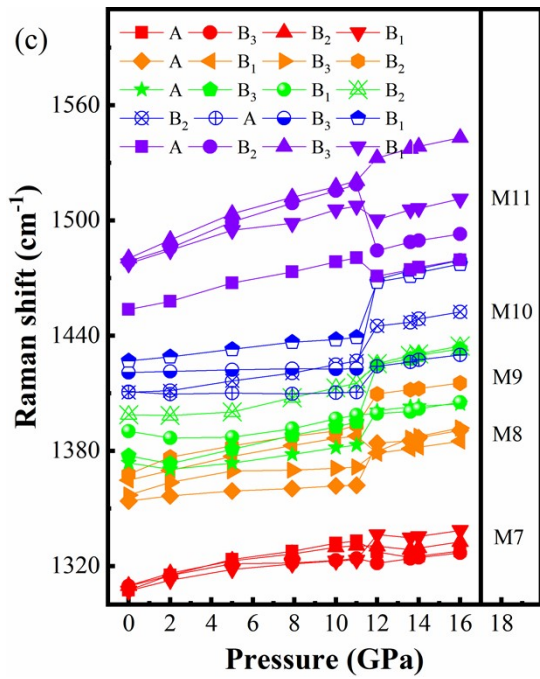
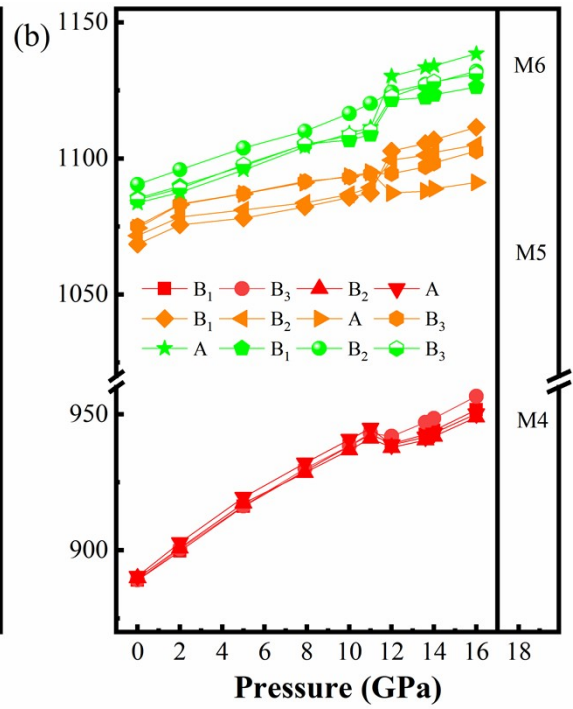
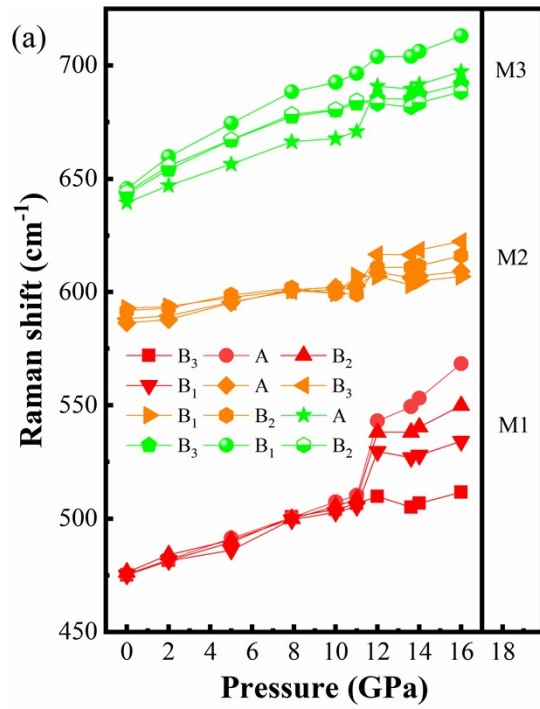
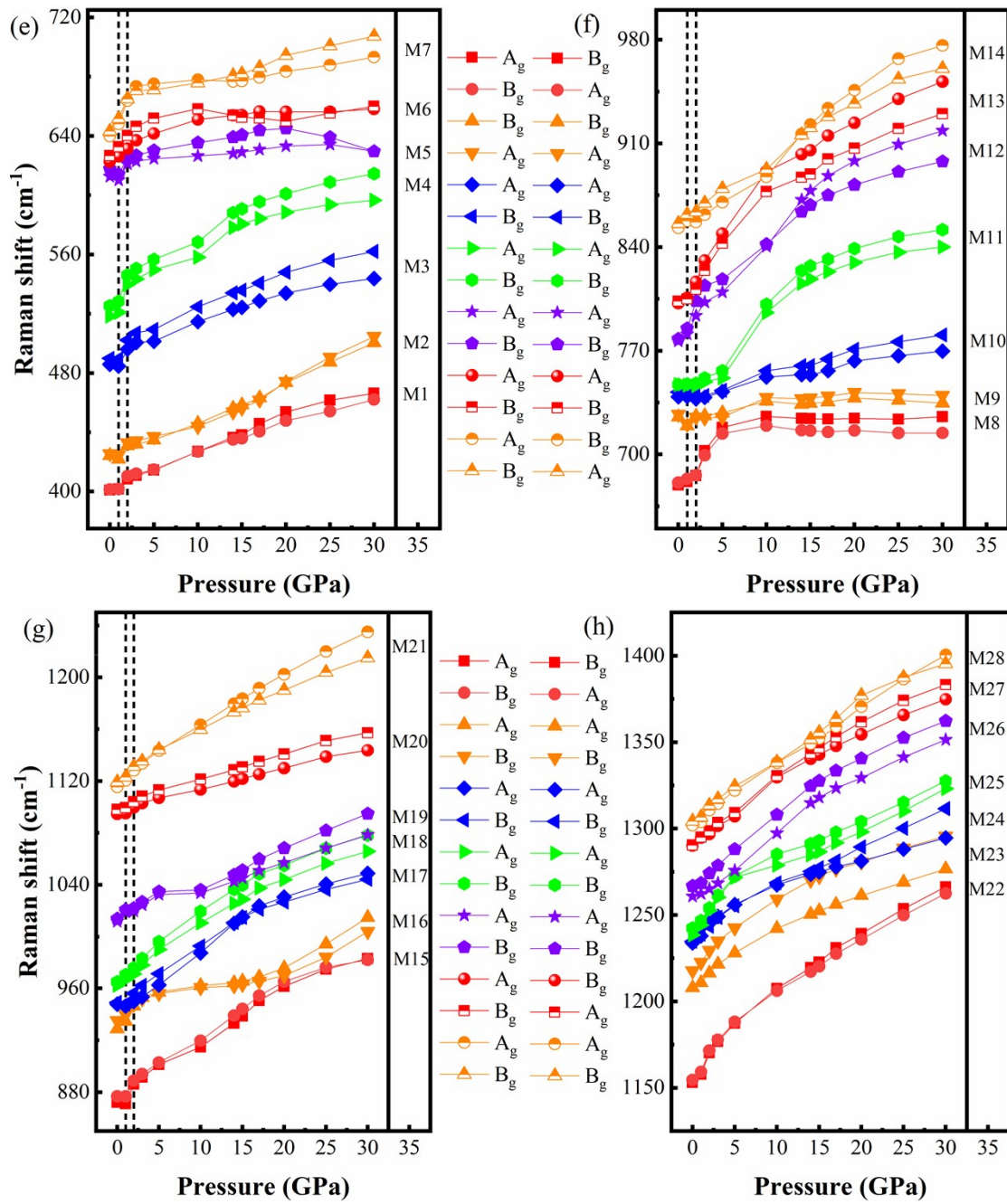


Fig. S3. The X-ray spectra of (a) NM and (b) NNHT change with the pressure.





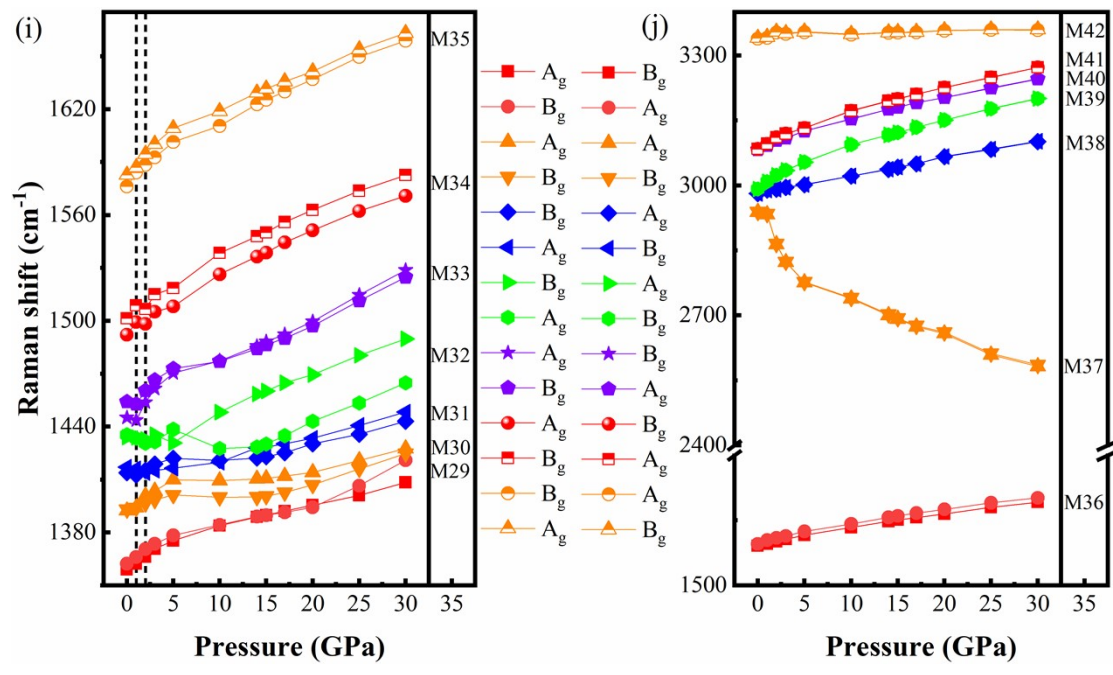
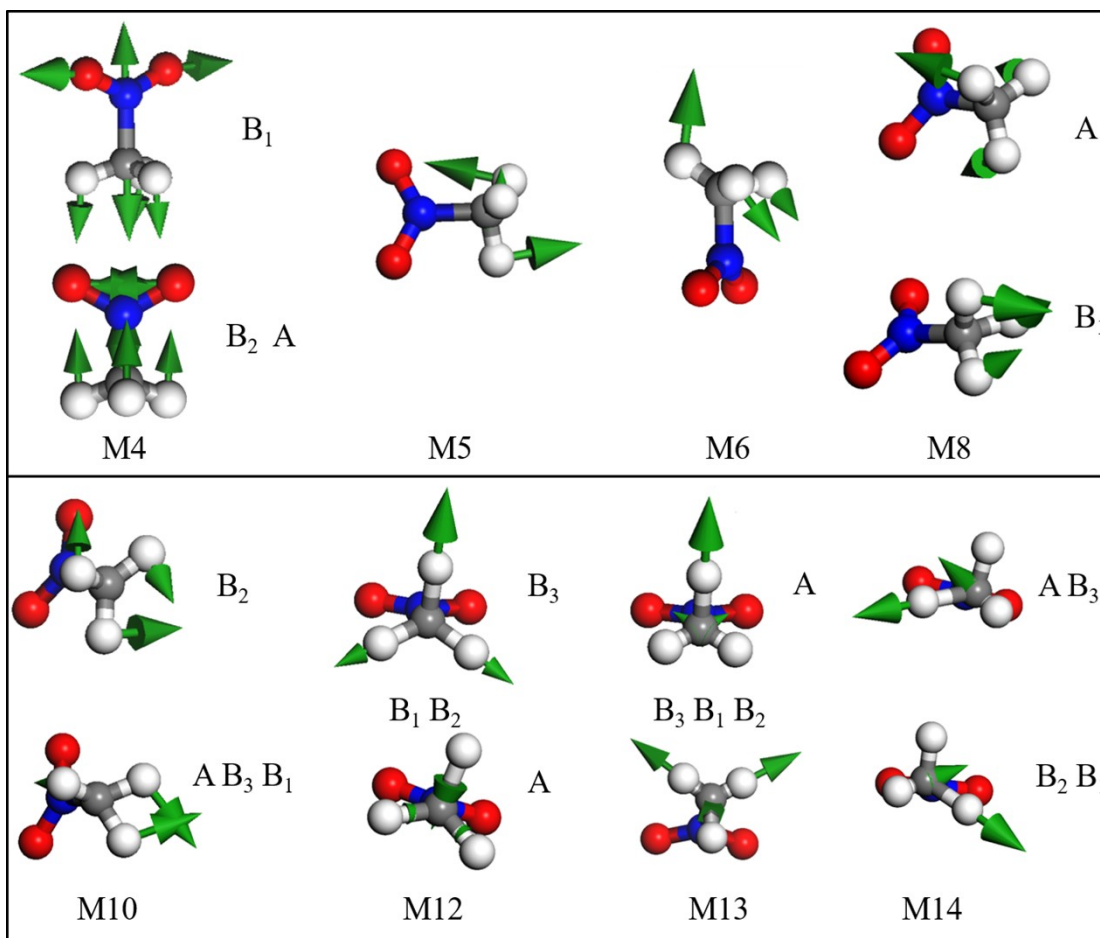
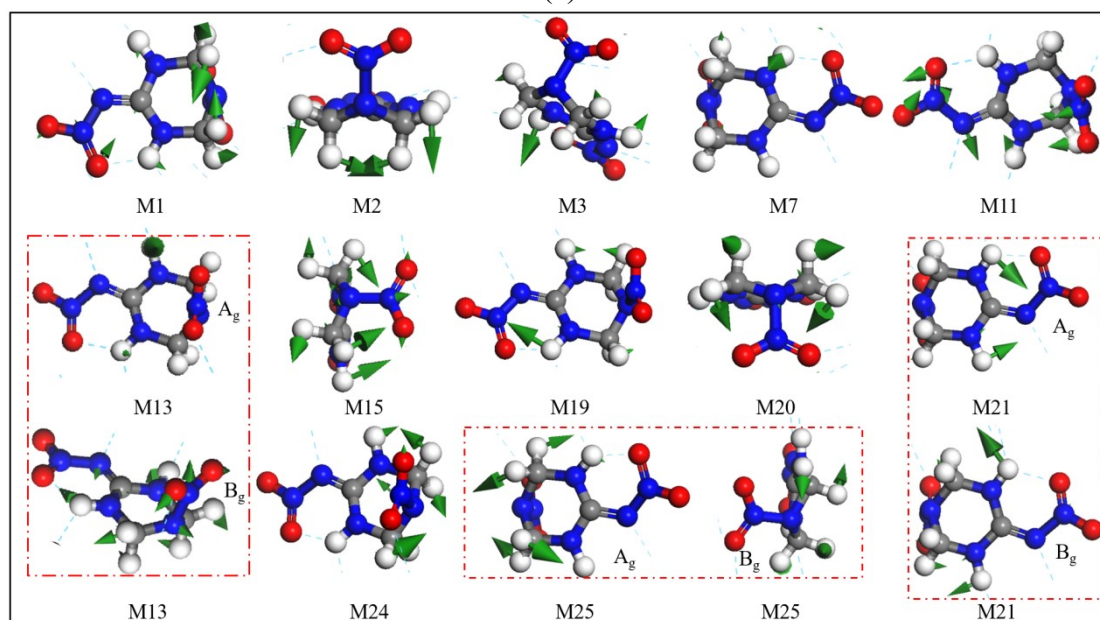


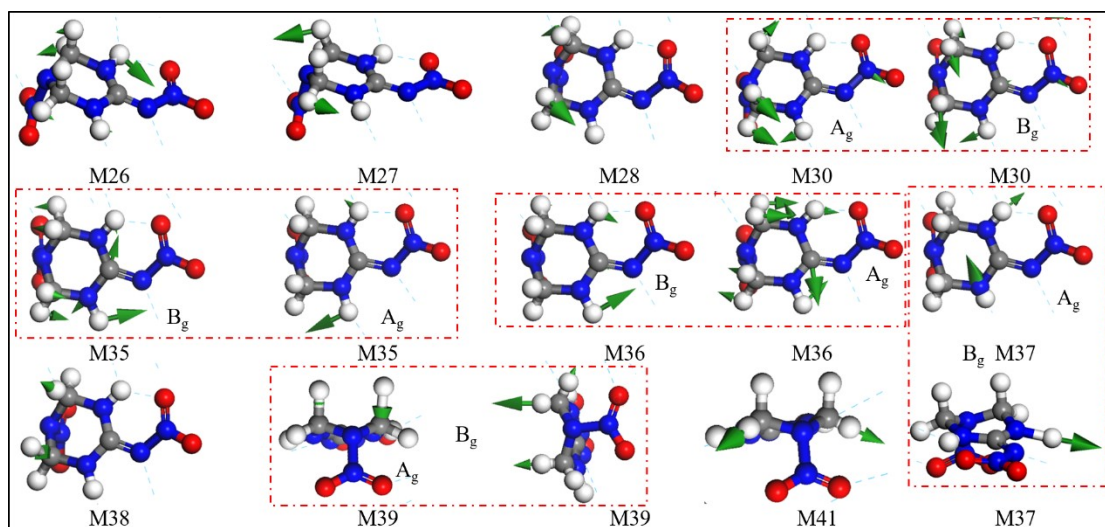
Fig. S4. The vibration frequency of NM and NNHT as a function of pressure. (a), (b), (c) and (d) belong to NM, (e), (f), (g), (h), (i) and (j) are NNHT.



(a)



(b)



(c)

Fig. S5. The states of the partial vibrational modes of the (a) NM and (b) (c) NNHT.

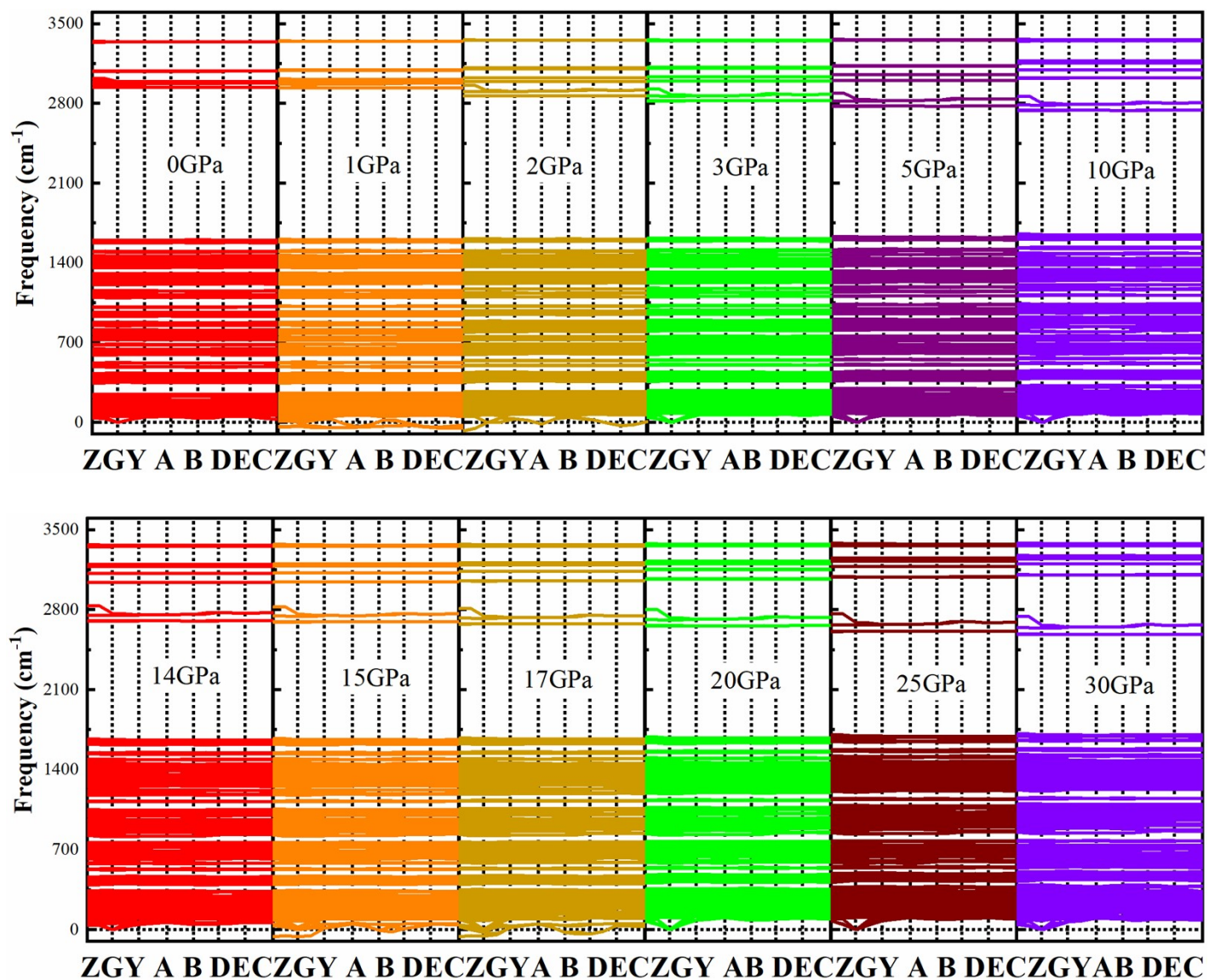


Fig. S6. Phonon dispersion spectra at different pressures of NNHT.

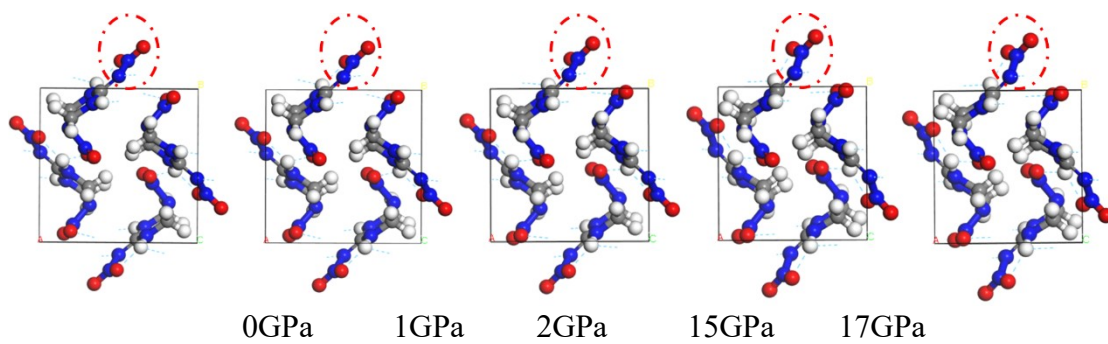


Fig. S7. Crystal structure projected along the YZ plane at several pressures of NNHT.

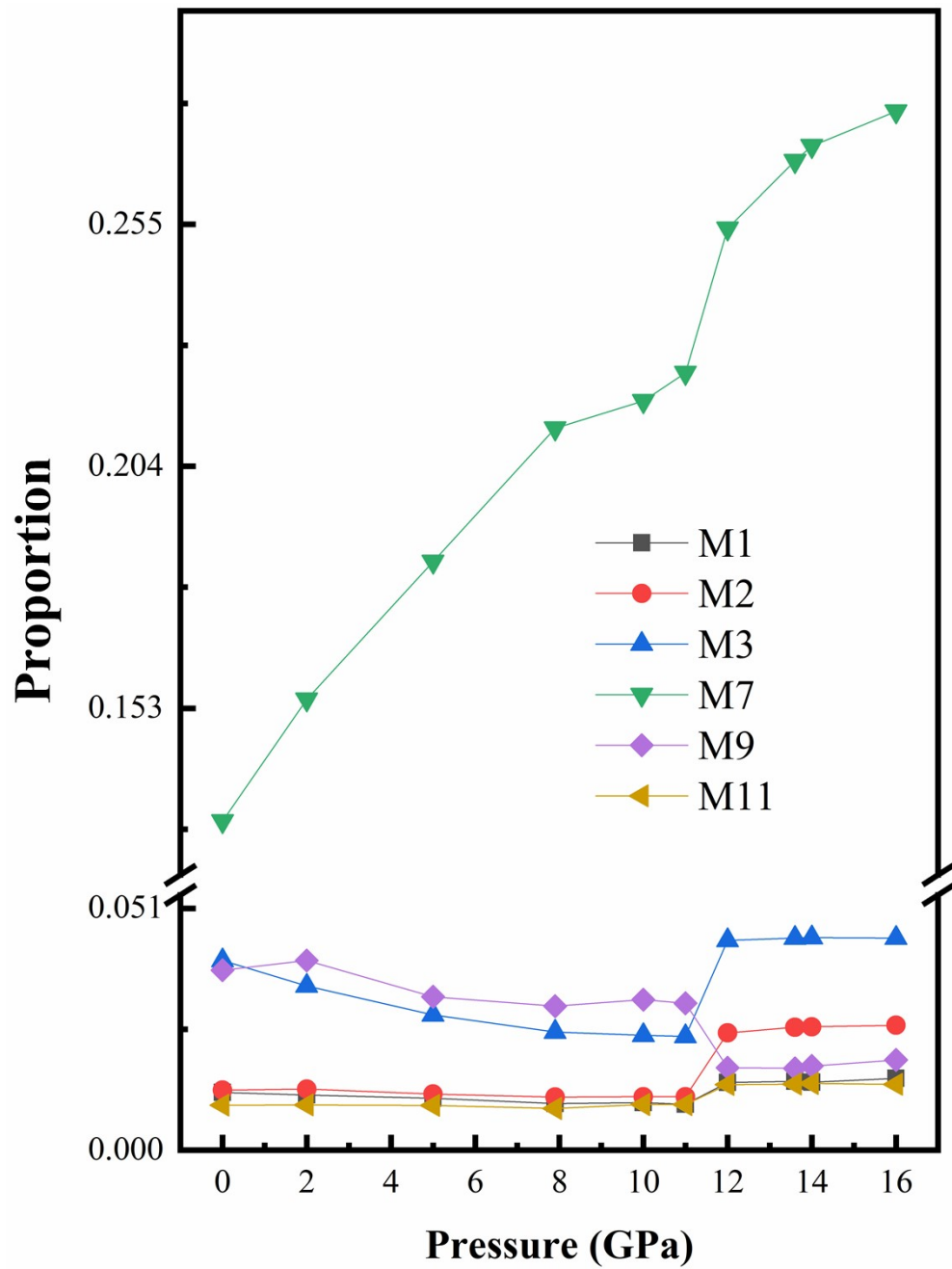


Fig.S8 The proportion of I_R / ν for NM as a function of pressure. As the detonation pressure approaches, the proportion of vibration modes increases gradually without the possibility of bond breaking.

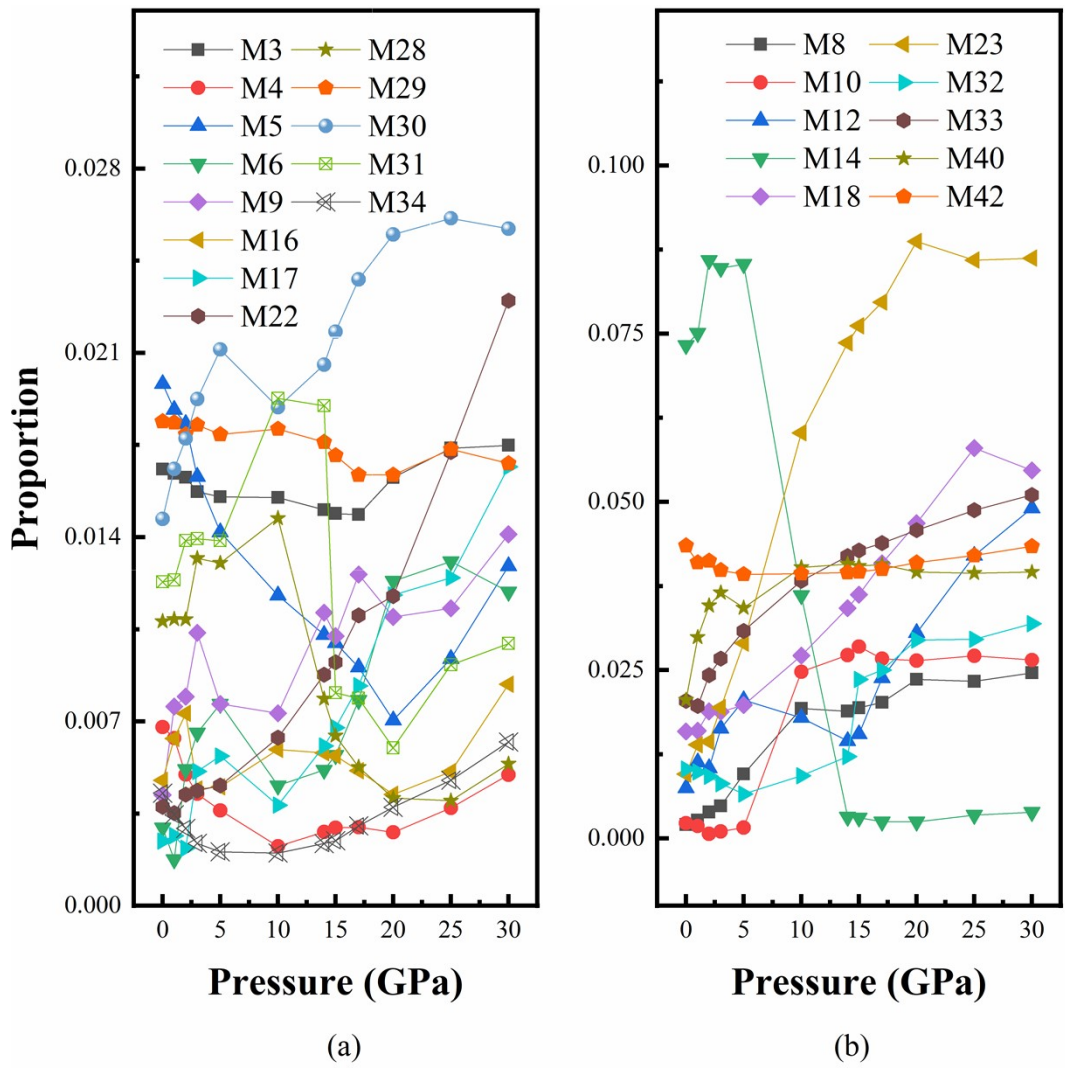


Fig.S9 The proportion of I_R / ν for NM as a function of pressure. As the detonation pressure approaches, the proportion of vibration modes increases gradually without the possibility of bond breaking.

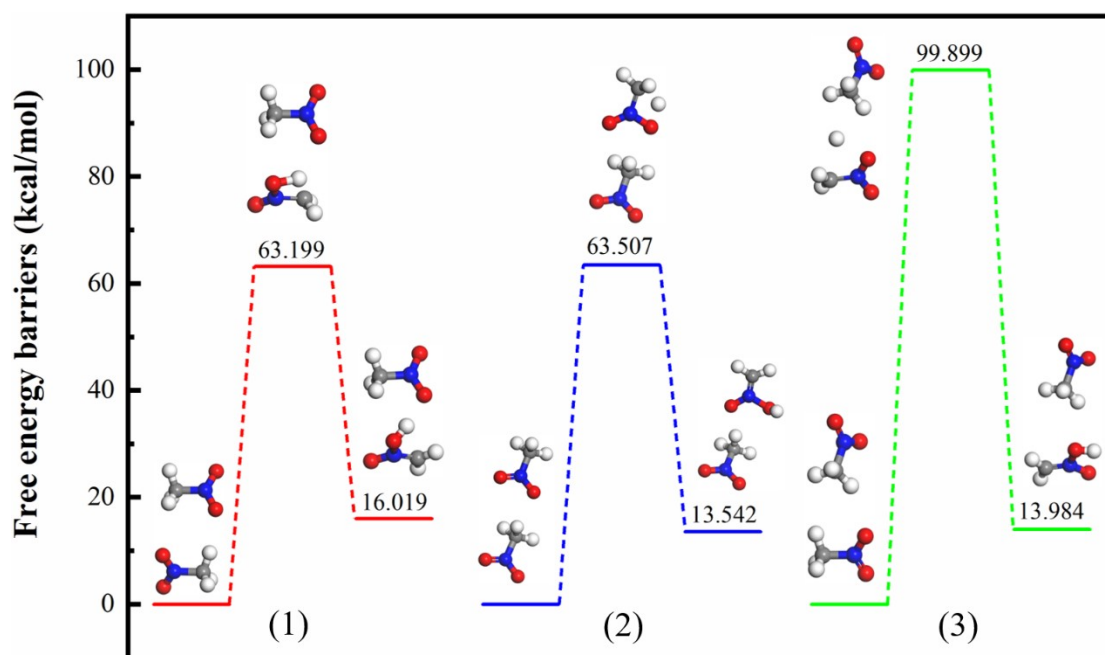


Fig.S10 The position distribution of possible reaction among the three kinds of NM molecules and the degree of difficulty of reaction.

Table S1 The calculated and experimental results of lattice parameters a (Å), b (Å), c (Å), β ($^\circ$) and V (Å³) of NM and NNHT.

Compound	Methods	Around	a	b	c	β	V	Ref.
NM	GGA-PBE-G	P=0, T=0	5.198	6.305	8.543		279.975	This work
	Neutron diffraction	T=4.2K	5.1832	6.2357	8.5181			[1]
		T=78K	5.1983	6.2457	8.5640			[1]
	X-ray diffraction	T=298k	5.197	6.292	8.747			[9]
	GGA-PBE	T=0K	5.317	6.754	8.980		322.49	[4]
	LDA-CAPZ	T=0K	4.91	6.03	8.10		239.82	[3]
	GGA-PW91		5.49	6.76	9.15		339.59	
	GGA-PBE		5.47	6.73	9.10		334.98	
	GGA-PB91-OBS		5.05	6.24	8.44		266.43	
	GGA-PBE-TS		5.21	6.48	8.64		291.97	
	GGA-PBE-G06		5.19	6.29	8.58		280.01	

	LDA-CAPZ	T=0K	4.882	6.029	8.153	239.96	[5]
	GGA-PBE		5.384	6.847	8.995	331.69	
	NPT-MD	T=4.2K	5.2116	6.3416	8.6464	285.766	[6]
		T=250.0K	5.2620	6.5691	8.9561	306.8167	
	ReaxFF MD	T=228K	5.223	6.275	8.604		[7]
		T=293K	5.231	6.284	8.617		
	GGA-PBE-G	T=0K	5.24593	6.32451	8.54383	283.456	[8]
NNHT	GGA-PBE-G	T=0K	8.801	8.781	9.319	89.222 720.112	This work
	GGA-PBE-TS	T=0K	8.849	8.890	9.467	90.422 744.384	This work
	X-ray diffraction		9.026	8.599	9.4038	91.199 729.7	[2]

Table S2 Calculated and experimental vibrational modes and frequencies of NM.

Mode	Sym.	This work	This work	Expt. [15]	GGA +PBE [4]	GGA+G06 [3]
		Assignments	Frequency (cm ⁻¹)			
M1	B ₃	CH ₃ + NO ₂ rocking	475.1	484.0		470.6
	B ₁		475.0	483.7	478	470.3
	A	CH ₃ + NO ₂ rocking	475.5	484.9		470.9
	B ₂	CH ₃ + NO ₂ rocking	476.4	484.1		472.7
M2	A	NCH ₃ wagging	586.4			585.9
	B ₃	NCH ₃ wagging	588.3	607.7	601	587.3
	B ₂		519.8	608.0		591.4
	B ₁	NCH ₃ wagging	592.9			592.4
M3	A	CN stretching + NO ₂ scissor	639.5			636.3

	B ₃	CN stretching + NO ₂ scissor	643.3		650	641.0
	B ₂		644.1	664.4		641.1
	B ₁	CN stretching + NO ₂ scissor	645.7	658.0		641.5
M4	B ₁	CN stretching + NO ₂ bending	889.0	922.0	906	889.1
	B ₃	CN stretching + NO ₂ bending	889.1			888.9
	B ₂	CN stretching + NO ₂ bending	889.8	923.8		889.9
	A	CN stretching + NO ₂ bending	890.5	923.6		890.1
M5	B ₁	CH ₃ twisting + NO ₂ antisymmetric stretching	1068.6	1106.1		1070.7
	B ₂	CH ₃ twisting + NO ₂ antisymmetric stretching	1071.6	1107.1	1083	1073.5
	A	CH ₃ twisting + NO ₂ antisymmetric stretching	1074.6	1105.3		1075.5
	B ₃	CH ₃ twisting + NO ₂ antisymmetric stretching	1075.3	1108.2		1076.7
M6	A	NCH ₃ deformation	1083.7			1088.3
	B ₃		1084.6	1124.3	1098	1089.5

	B ₁	NCH ₃ deformation	1085.5	1121.2		1090.5
	B ₂	NCH ₃ deformation	1090.5	1120.1		1095.4
M7	B ₁		1307.1	1379.3		1308.2
	A	CN stretching + CH ₃ deformation	1307.4	1375.4		1307.9
	B ₃	CH ₃ deformation +NO ₂ deformation	1309.6	1378.2	1342	1310.1
	B ₂	CH ₃ deformation +NO ₂ deformation	1309.8	1376.5		1310.3
M8	A	CH ₃ deformation + NO ₂ symmetric stretching	1353.9	1403.9	1387	1356.0
	B ₃		1357.0			1360.6
	B ₂		1367.9	1414.7		1371.4
	B ₁	CH ₃ deformation + NO ₂ symmetric stretching	1364.8			1368.2
M9	A	CH ₃ deformation	1373.8	1412.0		1381.3
	B ₃	CH ₃ deformation +NO ₂ antisymmetric stretching	1377.4	1413.6	1414	1384.1
	B ₂	CH ₃ deformation +NO ₂ antisymmetric stretching	1390.3	1414.1		1406.9

	B ₁	CH ₃ deformation +NO ₂ antisymmetric stretching	1398.8	1412.7		1396.6
M10	B ₂	CH ₃ deformation	1410.5	1430.9		1419.1
	A	CH ₃ deformation	1410.8		1434	1418.6
	B ₃	CH ₃ deformation	1420.8	1429.6		1429.3
	B ₁	CH ₃ deformation	1426.9			1434.5
M11	A	NO ₂ stretching + CH ₃ deformation	1453.6			1456.3
	B ₁		1477.5		1528	1480.1
	B ₂	NO ₂ antisymmetric stretching + CH ₃ deformation	1478.7	1565.4		1479.2
	B ₃	NO ₂ antisymmetric stretching + CH ₃ deformation	1480.4	1566.0		1483.1
M12	B ₃	CH ₃ symmetric stretching	2971.8			2981.0
	A	CH ₃ symmetric stretching	2972.2	2970.6	2980	2981.4
	B ₁	CH ₃ symmetric stretching	2972.8			2981.8
	B ₂	CH ₃ symmetric stretching	2974.1			2983.1

M13	B ₃	CH ₃ antisymmetric stretching	3077.7	3049.6		3081.2
	A	CH ₃ antisymmetric stretching	3078.1		3072	3080.9
	B ₁	CH ₃ antisymmetric stretching	3078.3			3081.6
	B ₂	CH ₃ antisymmetric stretching	3079.2			3082.7
M14	A	CH ₃ antisymmetric stretching	3124.7			3126.3
	B ₃	CH ₃ antisymmetric stretching	3124.8		3117	3126.5
	B ₂	CH ₃ antisymmetric stretching	3125.5	3082.2		3127.3
	B ₁	CH ₃ antisymmetric stretching	3126.1			3127.8

Table S3 Calculated vibrational modes and frequencies of NNHT.

Mode	Sym.	This work	This work
		Assignments	Frequency (cm ⁻¹)
M1	A _g	Ring deformation + NO ₂ + CH ₂ rocking in plane	400.9
	B _g	Ring deformation + CH ₂ + NO ₂ rocking in plane	401.4
M2	B _g	Ring deformation + CH ₂ rocking in plane	424.4
	A _g	Ring deformation + CH ₂ rocking in plane	425.6
M3	A _g	C-H + N-H + NO ₂ rocking in plane	485.9
	B _g	C-H + N-H + NO ₂ rocking in plane	490.0
M4	A _g	Ring deformation +C-H + NO ₂ rocking in plane	518.4
	B _g	Ring deformation +C-H+ NO ₂ rocking in plane	525.4
M5	A _g	Ring deformation + N-H rocking	612.6

	B _g		617.8
M6	A _g	Ring deformation + N-H rocking	622.7
	B _g	Ring deformation + N-H rocking	626.7
M7	A _g	Ring deformation + N-H rocking + C-H rocking	640.0
	B _g	Ring deformation + N-H rocking + C-H rocking	643.3
M8	B _g		679.3
	A _g	Ring deformation + N-H rocking + C=N rocking	681.0
M9	B _g	Ring deformation + CH ₂ rocking + NO ₂ rocking	725.3
	A _g	Ring deformation + CH ₂ rocking + NO ₂ rocking	727.0
M10	A _g	Ring deformation + N-H rocking + N-NO ₂ wagging out of plane	739.0
	B _g	Ring deformation + N-H rocking + N-NO ₂ wagging out of plane	742.1
M11	A _g	Ring deformation + CH ₂ translation + N-NO ₂ wagging out of plane + N-N twisting + N-H rocking	747.2
	B _g	Ring deformation + CH ₂ translation + N-NO ₂ wagging out of plane + N-N twisting + N-H rocking	747.4

M12	A _g	Ring deformation + N-H rocking	776.5
	B _g	Ring deformation + N-H rocking	778.0
M13	A _g	Ring deformation + N-H rocking	802.0
	B _g	Ring deformation + N-H rocking + NO ₂ scissors + CH ₂ rocking + N-NO ₂ (2) stretch	803.5
M14	B _g		853.1
	A _g	Ring deformation + N-H rocking + NO ₂ scissors + CH ₂ rocking + C=N twisting	856.0
M15	A _g	Ring deformation + N-H rocking + NO ₂ (2) scissors + CH ₂ rocking in plane + N-NO ₂ (2) stretch	872.2
	B _g	Ring deformation + N-H rocking + NO ₂ (2) scissors + CH ₂ rocking in plane + N-NO ₂ (2) stretch	876.8
M16	A _g	Ring deformation + N-H stretch + CH ₂ wagging out of plane	928.8
	B _g	Ring deformation + N-H bending + CH ₂ wagging out of plane	935.1
M17	A _g	Ring deformation + CH ₂ wagging in plane	947.8
	B _g	Ring deformation + CH ₂ wagging in plane	949.3
M18	A _g	N-CH ₂ stretch + N-N stretch + NO ₂ s-stretch	962.6

	B _g	N-CH ₂ stretch + N-N stretch + NO ₂ s-stretch	965.2
M19	A _g	Ring deformation + C-H + N-H wagging	1011.7
	B _g	Ring deformation + C-H + N-H wagging	1013.7
M20	A _g	Ring deformation + CH ₂ wagging	1094.5
	B _g	Ring deformation + CH ₂ wagging	1098.2
M21	A _g	Ring deformation + N-H wagging	1115.6
	B _g	Ring deformation + N-H wagging + CH ₂ wagging	1119.3
M22	B _g	Ring deformation + CH ₂ wagging out of plane + C-N bending	1153.1
	A _g	Ring deformation + CH ₂ wagging out of plane + C-N bending	1154.6
M23	A _g	Ring deformation + N-N bending + C-H wagging + NH wagging	1208.0
	B _g	Ring deformation + N-N bending + CH ₂ bending + NO ₂ stretch	1217.7
M24	A _g	Ring deformation + CH ₂ twisting + N-N stretch + NH wagging + NO ₂ bending	1233.9
	B _g	Ring deformation + CH ₂ twisting + N-N stretch + NH wagging + NO ₂ bending	1234.8

M25	A _g	Ring deformation + CH ₂ twisting + NH wagging	1238.6
	B _g	Ring deformation + CH ₂ twisting	1242.5
M26	A _g	Ring deformation + N-H wagging + CH ₂ wagging out of plane	1260.8
	B _g	Ring deformation + N-H wagging + CH ₂ wagging out of plane	1266.8
M27	A _g	Ring deformation + C-H wagging	1290.1
	B _g	Ring deformation + C-H wagging	1290.4
M28	A _g	Ring deformation + C-H wagging	1301.9
	B _g	Ring deformation + C-H wagging	1304.4
M29	A _g	Ring deformation + CH ₂ wagging out of plane	1358.9
	B _g	Ring deformation + CH ₂ wagging out of plane	1362.3
M30	A _g	Ring deformation + CH ₂ wagging out of plane + N-N wagging + NH wagging	1392.4
	B _g	Ring deformation + CH ₂ wagging out of plane + CH ₂ scissors + N-N wagging + NH wagging	1393.1
M31	B _g	Ring deformation + CH ₂ scissors + NH wagging	1413.8

	A _g	Ring deformation + CH ₂ scissors	1417.0
M32	B _g	Ring deformation + CH ₂ scissors + NH rocking	1434.1
	A _g	Ring deformation + CH ₂ scissors	1435.4
M33	A _g	Ring deformation + NH rocking	1445.1
	B _g	Ring deformation + NH rocking + CH ₂ scissors	1454.2
M34	A _g	Ring deformation + NO ₂ a- stretch + CH ₂ scissors	1492.1
	B _g	Ring deformation + NO ₂ a- stretch + NH wagging + CH ₂ scissors	1501.4
M35	B _g	Ring deformation + NH wagging + CH ₂ wagging + C-N stretch	1576.1
	A _g	Ring deformation + NH wagging	1582.8
M36	B _g	Ring deformation + NH wagging	1591.3
	A _g	Ring deformation + NH wagging + CH ₂ wagging out of plane + C-N stretch	1595.6
M37	A _g	Ring deformation + NH (2) stretch	2938.7
	B _g	Ring deformation + NH (2) stretch	2939.5

M38	A _g	CH ₂ stretch	2981.4
	B _g	CH ₂ stretch	2981.6
M39	A _g	CH ₂ stretch	2991.6
	B _g	CH ₂ stretch	2991.9
M40	B _g	CH ₂ s-stretch	3082.7
	A _g	CH ₂ s-stretch	3082.8
M41	B _g	CH ₂ s-stretch	3084.2
	A _g	CH ₂ s-stretch	3084.4
M42	A _g	NH (1) stretch	3338.9
	B _g	NH (1) stretch	3340.7

Table S4 Comparison of experimental and calculated values of partial bond lengths and BDEs for NM and NNHT.

Compound		Method	Bond length	BDE	Ref.
NM	C-N	GGA-PBE-G	1.499		Present
		B3LYP-G	1.498	62.792	Present
		B3LYP-6-13G*	1.498	56.4	[19]
		GGA	1.489		[4]
		Exp.		60.8	[25]
	Exp.	1.481		[1]	
	C-H3	GGA-PBE-G	1.098		Present
		B3LYP-G	1.087	98.968	Present
		GGA	1.090		[4]
		Exp.	1.098		[1]

	N-O2	B3LYP-G	1.221	123.183	
		GGA	1.225		[4]
		Exp.	1.223		[1]
NNHT	C1-N1	GGA-PBE-G	1.351		Present
		B3LYP-G	1.357	50.079	Present
		Exp.	1.325		[2]
	C1-N2	GGA-PBE-G	1.341		Present
		B3LYP-G	1.343	50.080	Present
		Exp.	1.325		[2]
	C2-H4	GGA-PBE-G	1.099		Present
		B3LYP-G	1.093	61.196	Present
		Exp.	1.00		[2]
	N3-N4	GGA-PBE-G	1.456		Present

	B3LYP-G	1.434	36.068	Present
	Exp.	1.416		[2]
N2-H2	GGA-PBE-G	1.025		Present
	B3LYP-G	1.017	102.515	Present
	Exp.	0.86		[2]
N6-O3	GGA-PBE-G	1.263		Present
	B3LYP-G	1.254	105.279	Present
	Exp.	1.243		[2]
